

ELECTRONIC SUPPLEMENTARY INFORMATION FOR

Determination of membrane capacitance and cytoplasm conductivity by the simultaneous electrorotation

Authors; Shikiho Kawai, Masato Suzuki, Satoshi Arimoto, Tsuguhiro Korenaga, Tomoyuki Yasukawa.

Table of Contents

Appendix A: Clausius-Mossotti factor of a single-shell model

Materials and Methods

Table S1: List of previously reported membrane capacitances and cytoplasm conductivities of various types of hematopoietic cells.

Figure S1: Schematic images of single-shell model of a cell.

Figure S2: Designs of IDA electrode substrates for the 3-D microelectrode device.

Figure S3: Dielectrophoretic behaviors of K562 cells.

Figure S4: Microscopic photographs of K562 cells injected in the device with 3D-IDA electrode at various concentrations.

Figure S5: Optical and fluorescent images of Jurkat cells that expressed the cell-surface antigen of CD7 and THP-1 cells.

Figure S6: Time-lapse images of the electrorotation of three microrods.

Movie S1: The simultaneous electrorotation of K562 cells by the 3D-IDA system.

Supporting References

Appendix A. Clausius-Mossotti factor of a single-shell model

A single-shell model is usually used for estimating an ac electrokinetic behavior (such as DEP and ROT) of a particle covered with a single layer of uniform thickness δ (in Fig. S1). In this model, the layered particle is replaced by an equivalent homogeneous particle. A complex permittivity of the equivalent homogeneous particle (ε_2^*) represented in Fig. S1 is given by (S1):¹

$$\varepsilon_2^* = \varepsilon_m^* \left[\frac{\left(\frac{R+\delta}{R}\right)^3 + 2 \frac{\varepsilon_i^* - \varepsilon_m^*}{\varepsilon_i^* + 2\varepsilon_m^*}}{\left(\frac{R+\delta}{R}\right)^3 - \frac{\varepsilon_i^* - \varepsilon_m^*}{\varepsilon_i^* + 2\varepsilon_m^*}} \right] \quad (\text{S1})$$

where, ε_m^* is the complex permittivity of shell and ε_i^* is the complex permittivity of particle interior. In the case of biological cells with the radius R and membrane thickness of δ , which is very thinner than R ($\delta \ll R$), the equation (S1) is simplified by adapting the binomial theorem as below.

$$(1 + \chi)^\alpha = 1 + \alpha\chi + \frac{\alpha(\alpha - 1)}{2!}\chi^2 + \dots \quad (\text{S2})$$

Thus, it can be approximated as follows.

$$\left(\frac{R+\delta}{R}\right)^3 = \left(1 + \frac{\delta}{R}\right)^3 \approx 1 + 3\frac{\delta}{R} \quad (\text{S3})$$

From eqs (S1) and (S3), the complex permittivity of the cell can be written as

$$\varepsilon_2^* = \frac{C_m R(j\omega\tau_i + 1)}{j\omega(\tau_m + \tau_i) + 1} \quad (\text{S4})$$

Furthermore, the membrane conductivity is assumed to be negligible. Using equation (S4), the complex Clausius-Mossotti factor becomes

$$CM = -\frac{\omega^2(\tau_1\tau_m - \tau_i\tau'_m) + j\omega(\tau'_m - \tau_1 - \tau_m) - 1}{\omega^2(\tau_i\tau'_m + 2\tau_1\tau_m) - j\omega(\tau'_m + 2\tau_1 + \tau_m) - 2} \quad (4)$$

Materials and Methods

Experiments for the dielectrophoresis

A conventional IDA electrode, which consisted of microband electrodes with 20 μm in width and 50 μm in gaps was used to observe dielectrophoretic behavior of cells. The IDA electrode was mounted on a glass substrate through the spacer with 30 μm thickness. Cells suspended in ROT solution were injected in the space between the upper IDA electrode and the lower glass substrate. An AC signal with opposite phase was then applied to microband electrodes to estimate the arrived positions of cells. The voltage of 5 V_{pp} with different frequencies from 0.1 MHz to 2.0 MHz was applied. The dielectrophoretic behavior of cells is accounted as negative dielectrophoresis (n-DEP) when cells arrived under the each microband electrodes, and accounted as positive-DEP (p-DEP) when cells are attached to edges of microband electrodes.

Table S1. List of reported previously membrane capacitances and cytoplasm conductivities of various types of hematopoietic cells.

Cell type	Radius [μm]	Membrane capacitance [mF m^{-2}]	Cytoplasm conductivity [S m^{-1}]	Method	Ref
T-Lymphocytes					
Jurkat	7.6 \pm 0.1	7.1	0.41 - 0.82	ROT	2)
Jurkat	7.4	13.5 - 14	0.84 - 1.1	ROT	3)
Jurkat	8.7 \pm 0.1	8.4 - 11	0.26 - 0.38	ROT	4)
Jurkat	7.2 \pm 0.85	15 \pm 1	-	patch-clamp	5)
T-lymphocyte (human)	3.04 \pm 0.26	12.1	1.06 - 1.1	ROT	6)
T-lymphocyte (human)	3.29 \pm 0.35	10.5 \pm 3.1	0.65 \pm 0.15	ROT	7)
T-lymphocyte (human)	3.6 \pm 0.55	7.01 \pm 0.91	0.53 \pm 0.1	ROT (3D octode)	8)
T-lymphocyte (human)	4.75 \pm 0.12	8.05 \pm 0.47	0.5	ROT Array	9)
Monocytes					
THP-1	7.3 \pm 0.966	17.19	0.0104	DEP	10)
THP-1	8	4.0	0.109	DEP	11)
Monocyte (human)	4.63 \pm 0.36	15.3 \pm 4.3	0.56 \pm 0.10	ROT	7)
Monocyte (human)	4.8 \pm 0.55	11.77 \pm 2.12	0.37 \pm 0.15	ROT (3D octode)	8)
Erythroleukaemia					
K562	-	2.0 \pm 1.0	0.15 \pm 0.05	DEP	12)
K562	10	2.7 \pm 0.8	0.2	cell rotation	13)
K562	4	8.2	0.21 - 0.24	DEP	14)
K562	-	9.7	0.28	DEP	15)
K562	6 \pm 1	8.93 \pm 1.43	0.32 \pm 0.08	ROT	16)
DS19 (murine erythroleukaemia)	5.4	17.4 \pm 2.0	0.8 - 1.1	ROT	17)
B-lymphocytes					
B-lymphocyte (human)	3.29 \pm 0.26	12.6 \pm 3.5	0.73 \pm 0.18	ROT	7)
B-lymphocyte (human)	3.6 \pm 0.6	10.33 \pm 1.6	0.41 \pm 0.1	ROT (3D octode)	8)
B-lymphocyte (human)	4.1 \pm 0.7	10.14 \pm 0.08	0.55 \pm 0.07	3D ROT	18)

Figure S1. Schematic images of single-shell model of a biological cell.

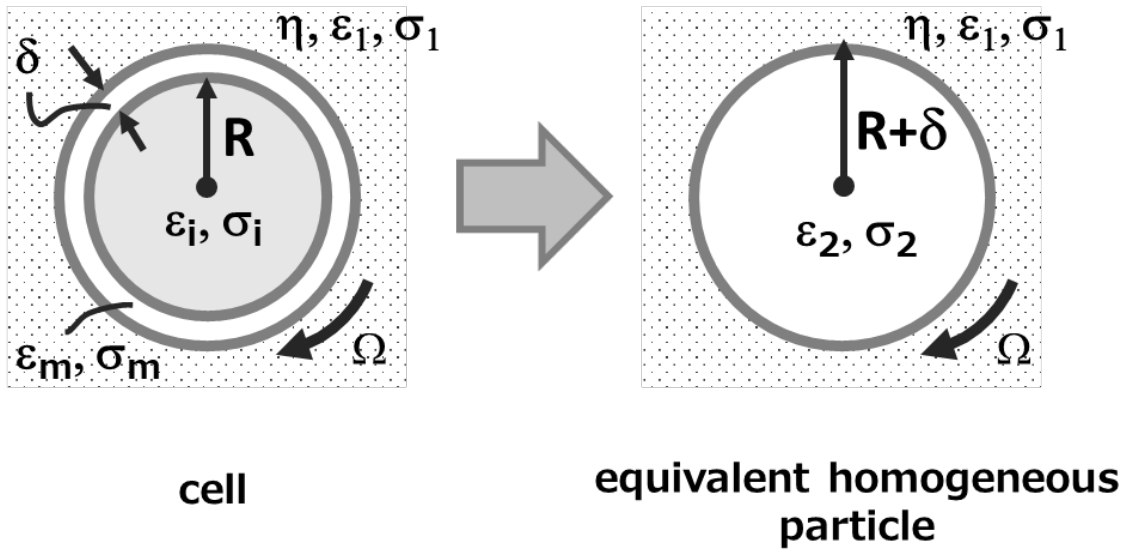


Figure S2. Designs of IDA electrode substrates for the 3-D IDA device. Schematic images and microscopic images of (A) horizontal and (B) vertical electrode patterns. The gap and width of each microband electrode are set to 30 μm and 20 μm , respectively. (C) Photo of the whole device.

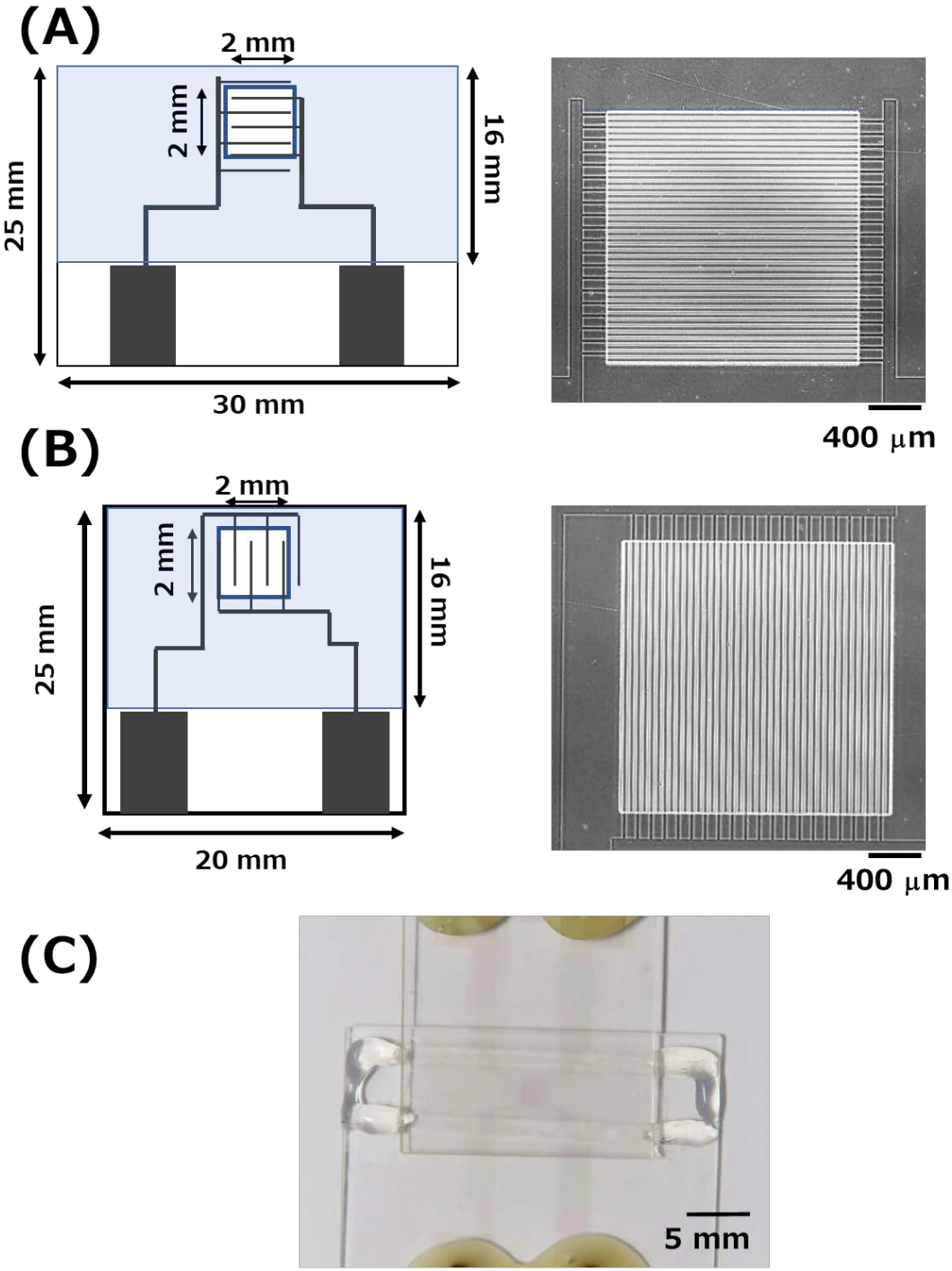


Figure S3. Dielectrophoretic behaviors of K562 cells when AC voltage with the frequency region (A) from 1.2 MHz to 2 MHz and (B) from 0.1 MHz to 1.1 MHz was applied to the microband electrodes of IDA. K562 cells moved (A) to the edge of the microband electrodes by the attractive force of positive dielectrophoresis and (B) below the microband electrodes by the repulsive force of negative dielectrophoresis to form a line pattern.

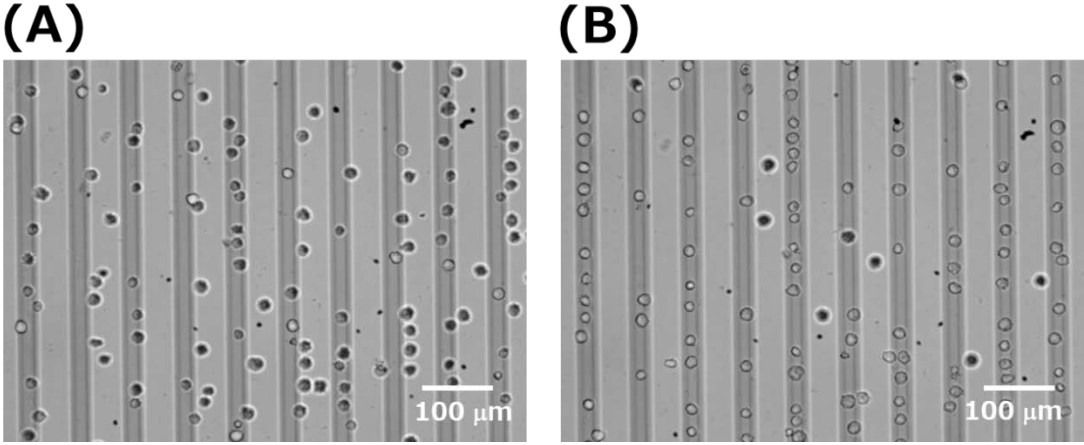


Figure S4. Microscopic photographs of K562 cells injected in the device with 3D-IDA electrode at various concentrations. (A) 0.5×10^7 cells mL^{-1} , (B) 1.0×10^7 cells mL^{-1} , (C) 2.0×10^7 cells mL^{-1} , (D) 8.0×10^7 cells mL^{-1} , and (E) 16×10^7 cells mL^{-1} .

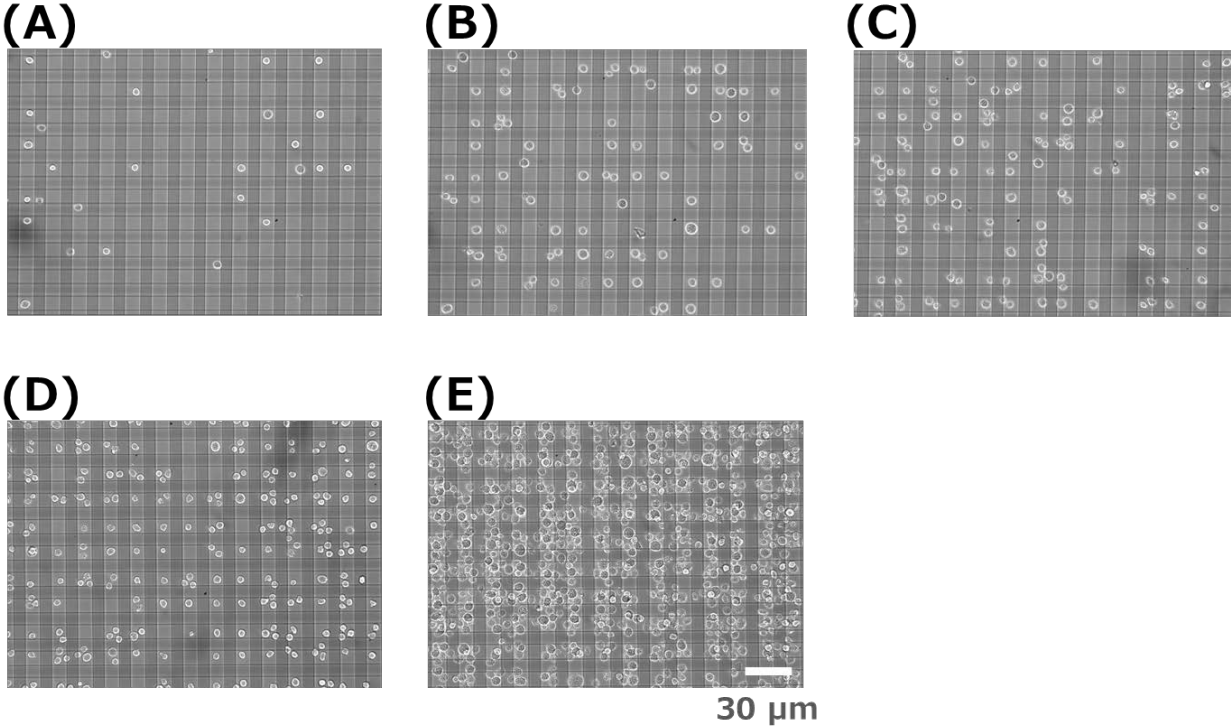


Figure S5. Optical and fluorescent images of Jurkat cells that expressed the cell-surface antigen of CD7 and THP-1 cells. Both types of cells were treated by the anti-CD7 antibody labeled with PE. Red fluorescence was observed from Jurkat cells, while no fluorescence was observed from THP-1.

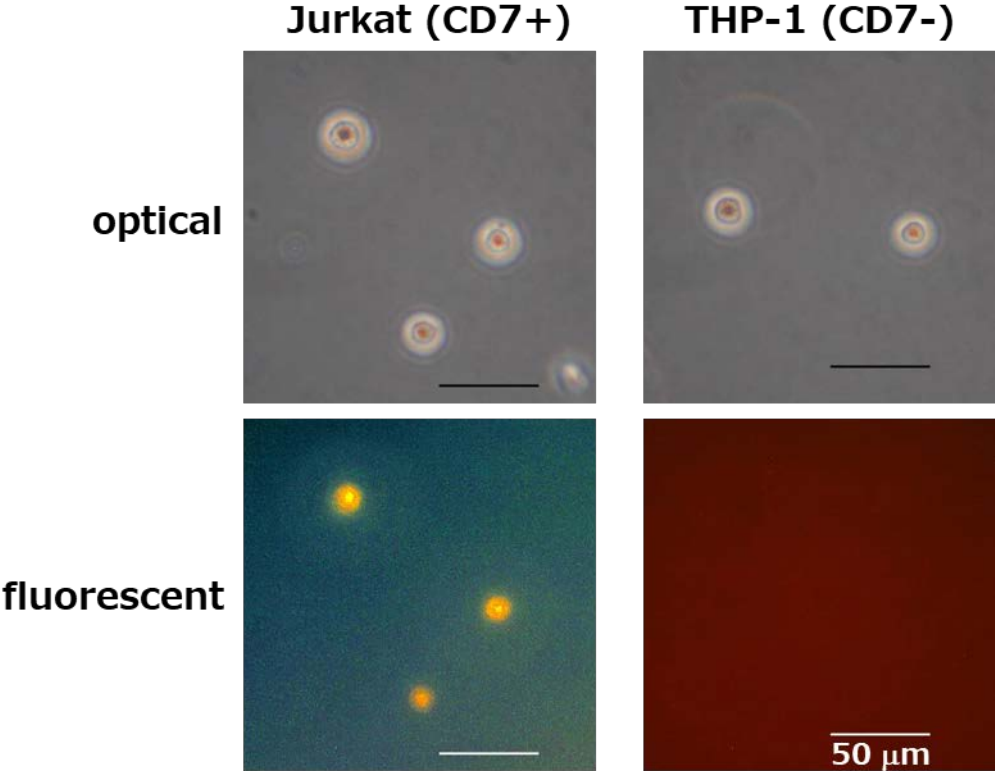
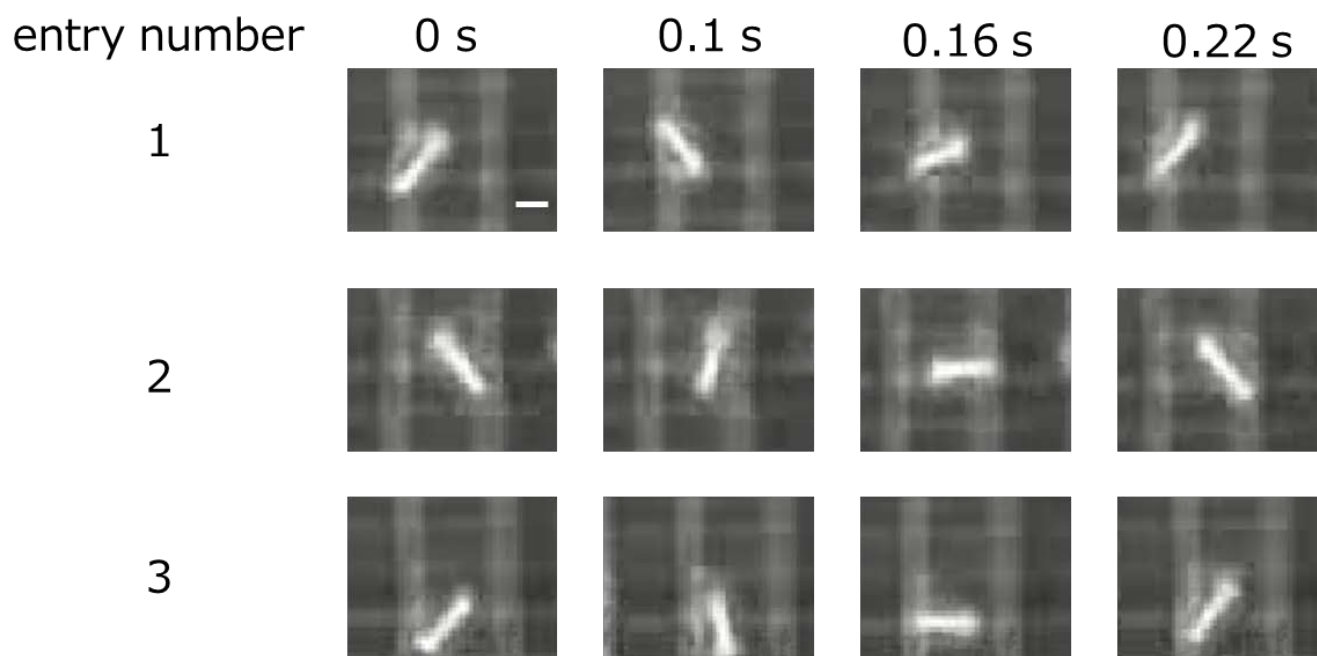


Figure S6. Time-lapse images of the electrorotation of three microrods. The scale bar represents 10 μm . The rotation rates of microrods of entry 1, 2, and 3 were 16.9, 15.7 and 15.2 radian s^{-1} , Respectively. The microrods of entry 1 and 3 were rotated to clockwise direction, while the rod of entry 2 was rotated opposite direction.



Supporting References

- 1 T. B. Jones, *Electromechanics of Particles*, Cambridge University Press, Cambridge, 1995.
- 2 V. L. Sukhorukov, M. Kürschner, S. Dilsky, T. Lisec, B. Wagner, W. A. Schenk, R. Benz and U. Zimmermann, *Biophys. J.*, 2001, **81**, 1006–1013.
- 3 M. Kiesel, R. Reuss, J. Endter, D. Zimmermann, H. Zimmermann, R. Shirakashi, E. Bamberg, U. Zimmermann and V. L. Sukhorukov, *Biophys. J.*, 2006, **90**, 4720–9.
- 4 V. L. Sukhorukov, D. Imes, M. W. Woellhaf, J. Andronic, M. Kiesel, R. Shirakashi, U. Zimmermann and H. Zimmermann, *Biochim. Biophys. Acta - Biomembr.*, 2009, **1788**, 1841–1850.
- 5 P. E. Ross, S. S. Garber and M. D. Cahalan, *Biophys. J.*, 1994, **66**, 169–78.
- 6 Y. Huang, X. B. Wang, P. R. C. Gascoyne and F. F. Becker, *Biochim. Biophys. Acta - Biomembr.*, 1999, **1417**, 51–62.
- 7 J. Yang, Y. Huang, X. Wang, X.-B. Wang, F. F. Becker and P. R. C. Gascoyne, *Biophys. J.*, 1999, **76**, 3307–3314.
- 8 S.-I. Han, Y.-D. Joo and K.-H. Han, *Analyst*, 2013, **138**, 1529.
- 9 K. Keim, M. Z. Rashed, S. C. Kilchenmann, A. Delattre, A. F. Gonçalves, P. Éry and C. Guiducci, *Electrophoresis*, 2019, **40**, 1830–1838.
- 10 M. B. Sano, E. A. Henslee, E. Schmelz and R. V. Davalos, *Electrophoresis*, 2011, **32**, 3164–3171.
- 11 R. Mohamed, M. Azhar Abdul Razak and N. Adib Kadri, *Biomed. Res. Ther.*, 2019, **6**, 3040–3052.
- 12 T. L. Mahaworasilpa, H. G. L. Coster and E. P. George, *Biochim. Biophys. Acta - Biomembr.*, 1994, **1193**, 118–126.
- 13 T. L. Mahaworasilpa, H. G. L. Coster and E. P. George, *Biochim. Biophys. Acta - Biomembr.*, 1996, **1281**, 5–14.
- 14 F. H. Labeed, H. M. Coley, H. Thomas and M. P. Hughes, *Biophys. J.*, 2003, **85**, 2028.
- 15 F. H. Labeed, H. M. Coley and M. P. Hughes, *Biochim. Biophys. Acta - Gen. Subj.*, 2006, **1760**, 922–929.
- 16 G. Bahrieh, M. Erdem, E. Özgür, U. Gündüz and H. Külah, *RSC Adv.*, 2014, **4**, 44879–44887.
- 17 X. B. Wang, Y. Huang, P. R. C. Gascoyne, F. F. Becker, R. Hölzel and R. Pethig, *BBA - Biomembr.*, 1994, **1193**, 330–344.
- 18 L. Huang, P. Zhao and W. Wang, *Lab Chip*, 2018, **18**, 2359–2368.